# Thermal Vacuum Testing of Advanced Thermal Control Devices for Flight Demonstration

Satoshi Kajiyiama[1], Takuji Mizutani[1], Takuya Ishizaki[1], Kota Tomioka[2], and Hosei Nagano[3]
*Nagoya University, Furo-cho, Nagoya, 464-8603, Japan*

Hiroto Tanaka[4] and Hiroki Nagai[5]
*Tohoku University, Sendai, 980-8577, Japan*

Kan Matsumoto[6]
*WEL Research Co. Ltd., Ichihara, 299-0102, Japan*

Kenichiro Sawada[7]
*Japan Aerospace Exploration Agency, Sagamihara, 305-8505, Japan*

Yoshihiro Machida[8]
*Shinko Electric Industries Co. Ltd., Kita-Owaribe, Nagano, 381-0014, Japan*

Kazuaki Matsumoto[9]
*Tochigi Kaneka corporation, Mohka, 321-4367, Japan*

**Abstract**

In this paper, the test results of the thermal vacuum testing of advanced thermal control devices (ATCD) are presented. ATCD consists of two types of flexible thermal straps: one is made of high-thermal-conductive material, and the other is made of a loop heat pipe, and a re-deployable radiator. The conductive-type thermal-strap (CTS) is made of high-thermal-conductive graphite-sheets and aluminum blocks. The LHP-type thermal-strap (LTS) is made of a ultrathin loop heat pipe. The reversible thermal panel (RTP) is made of high-thermal-conductive graphite-sheets as a flexible fin, and a shape-memory-alloy as a passive re-deployable actuator. It was confirmed that the thermal conductance between the two ends of CTS was 0.50-0.55 W/K. As for LTS, it was confirmed that it could operate even after recovering from the frozen condition of the working fluid, and that there was no leakage of the working fluid and no performance degradation under vacuum environment. As the heat load increased, the thermal conductance between the evaporator and condenser increased,

[1] Graduate student, Department of Mechanical System Engineering, Furo-cho, Chikusa-ku, Nagoya, Aichi, 464-8603, Japan
[2] Postdoctoral researcher, Department of Mechanical System Engineering, Furo-cho, Chikusa-ku, Nagoya, Aichi, 464-8603, Japan
[3] Professor, Department of Mechanical System Engineering, Furo-cho, Chikusa-ku, Nagoya, Aichi, 464-8603, Japan
[4] Graduate student, Department of Aerospace Engineering, 2-1-1, Katahira, Aoba-ku, Sendai, Miyagi 980-8577, Japan
[5] Professor, Institute of Fluid Science, 2-1-1, Katahira, Aoba-ku, Sendai, Miyagi 980-8577, Japan
[6] Engineer, Space Development Engineering Division, 2-12-11, Aoyagi, Ichihara-Shi, Chiba, 299-0102, Japan
[7] Associate Senior Researcher, Research Unit II, Research and Development Directorate, 2-1-1, Sengen, Tsukuba, Ibaraki, 305-8505, Japan
[8] Researcher, Shinko Electric Industries co, ltd., 36, Kita-Owaribe, Nagano, 381-0014, Japan
[9] Researcher, Tochigi Kaneka corporation, 14, Kinugaoka, Mohka, Tochigi, 321-4367, Japan

and finally a thermal conductance value of 4.1 W/K (at 5 W heat load) was confirmed. For RTP, it was confirmed that the radiator fins were fully expanded to 130° when the SMA actuator reached 30 ℃ during heating. On the other hand, during cooling, the temperature of the SMA actuator dropped only to -15℃, and the fins retracted only to 40°. Furthermore, the temperature hysteresis of the SMA actuator was estimated to be about 40℃ based on the experimental results.

## Nomenclature

$G_{CTS}$: Thermal conductance between both sides of conductivity-type thermal strap

$G_{LTS}$: Thermal conductance between LHP-evaporator and LHP-condenser

$Q_{CTS}$: Heat input on conductivity-type thermal strap

$Q_{EVA}$: Heat input on evaporator of LHP-type thermal strap

$T_C$: Temperature on hot side of conductivity-type thermal strap

$T_{CON}$: Temperature on condenser of LHP-type thermal strap

$T_{EVA}$: Temperature on evaporator of LHP-type thermal strap

$T_H$: Temperature on cold side of conductivity-type thermal strap

*Acronym*

CTS: Conductivity-type thermal strap

GFRP: Glass fiber reinforced plastics

LTS: LHP-type thermal strap

RTP: Reversible thermal panel

SMA: Shape memory allow

## I. Introduction

In current space development, innovative improvements in thermal control technology are strongly desired as spacecraft become more sophisticated. In particular, the development of lightweight, power-saving, and highly efficient thermal control devices is urgently required as spacecraft become smaller. The effectiveness of these devices has been confirmed on the ground level. On the other hand, opportunities for on-orbit demonstrations are very limited, and there are many thermal control devices that have not been tested in flight. Therefore, in order to obtain the opportunity to demonstrate such thermal control devices in orbit, we developed the Advanced Thermal Control Device (ATCD), which is a component of several thermal control devices that can be installed in the Innovative Satellite Technology Demonstration Program. The Innovative Satellite Technology Demonstration Program, which provides space demonstration opportunities for instruments and nano-satellites developed by private companies and universities, is being implemented by JAXA. So far, the first innovative satellite technology demonstration satellite was launched in January 2019. The second satellite was launched in FY2021, and 14 demonstration themes have been adopted. One of the components is the ATCD. This paper reports on the development and evaluation of the ATCD.

## II. Specifications of Advanced Thermal Control Device

The ATCD consists of three devices: a conductivity-type thermal strap (CTS) made of Kaneka graphite sheets, a LHP-type thermal-strap (LTS) made of a ultra-thin loop heat pipe[3], and a reversible thermal panel (RTP)[4].

Figure. 1 shows the external and internal images of the ATCD, which has a box-shaped enclosure made of A5052. LTS and CTS are attached to the sides of the enclosure to transport the heat from the simulated heat source to the top surface. The RTP is attached to the top surface and dissipates the heat transported by the LTS and the CTS by changing the deployment angle according to the temperature. The details of each device are described next.

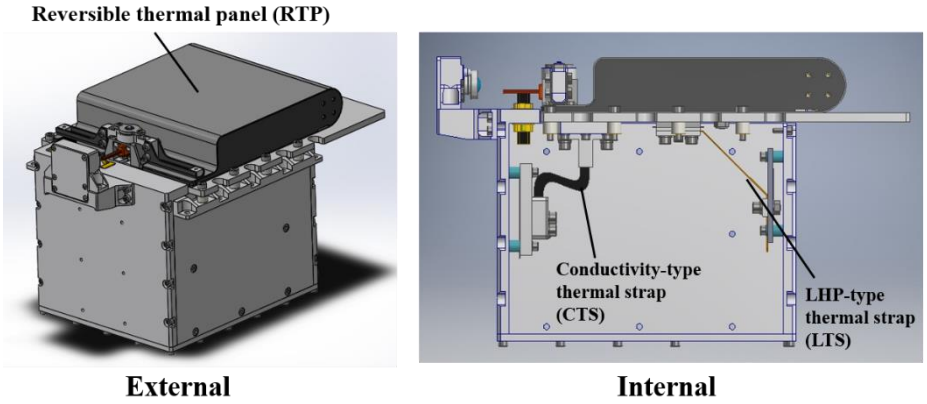


Fig. 1 External and internal images of ATCD

### A. Conductivity-type thermal strap (CTS)

The conductivity-type thermal strap (CTS; Fig. 2) is made of 150 layers of Kaneka graphite sheets[5] with a thermal conductivity of about 1200 W/mK and a thickness of 40 μm. The strap is not bonded between the layers to ensure flexibility, and the ends are fixed with aluminum brackets sandwiched and crimped to ensure heat transfer in the layer direction. The outermost layer of the strap is covered with a polyimide film for mechanical strength and corrosion resistance. In the on-orbit test, we will verify that the performance is equivalent to the ground test.

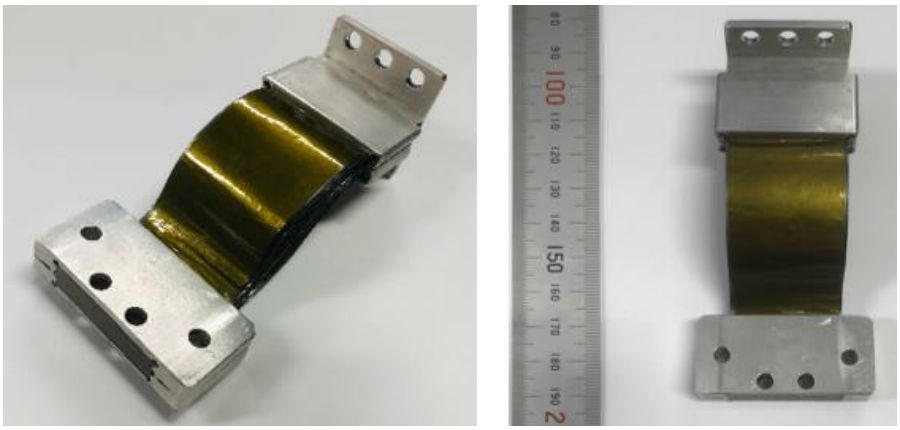

Fig. 2 Photos of conductivity-type thermal strap

### B. LHP type thermal strap (LTS)

The LHP-type thermal strap (LTS; Fig. 3) is a smaller and thinner version of the loop heat pipe (LHP) [6], which is a vapor-liquid two-phase heat transport device. The LTS is made of copper with a thickness of 0.6 mm and total weighs only about 11 g. Compared with conventional thermal straps that use only heat conduction between materials, the LHP uses latent heat transport by a working fluid inside the LHP, which is expected to have a high thermal conductance. After the working fluid is charged from the charging port near the liquid pipe, the working fluid is sealed by crimping and crushing the charging port. In addition, as shown in the right figure of Fig. 3, it is flexible because it can be bent without blockage of the flow path.

The LHP-type thermal strap installed in the ATCD uses water as the working fluid, which has never been demonstrated in space before. Therefore, we will verify whether the working fluid does not leak, whether it can be thawed, and whether it can be operated without any problem after thawing.

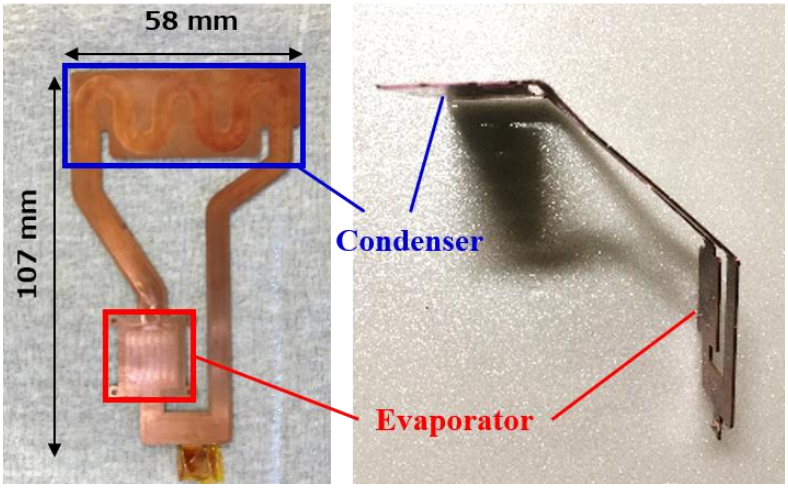


Fig. 3 Pictures of LHP-type thermal strap

### C. Reversible thermal panel (RTP)

The RTP (Fig. 4) is a radiator that enhances heat dissipation by expanding the heat-dissipating surface when the heat source is hot, and reduces heat dissipation by retracting the heat-dissipating surface when the heat source is cold. The RTP is characterized by its ability to handle a wide range of heat input without power by using SMA for deployment and stowage. SMA is mainly alloys of Ti and Ni, with a martensitic phase below a certain temperature (transformation temperature) and an austenitic phase above the transformation temperature. SMA has a shape memory effect in that it recovers its original shape when heated to the austenite phase after deformation in the martensite phase, and a superelastic effect in that the martensite phase has low stiffness and is easily deformed, while the austenite phase has high stiffness and is not easily deformed. SMA by itself has the unidirectional property of returning to its original shape above the transformation temperature, but by combining a torsion spring, SMA that has returned to its original shape above the transformation temperature can be deformed again below the transformation temperature. RTP is equipped with this type of SMA actuator. Since the SMA actuator uses the deformation of the member itself as the actuator, it has a simple structure and can be used in environments where electric actuators cannot be incorporated.

The RTP on ATCD is made of laminated Kaneka graphite sheets on the panel surface and laminated CFRP on the panel sides to maintain the structure, and the surface and back of the panel are coated with silver coated Teflon. The surface and back of the panels are coated with silver-deposited Teflon. The mass of overall RTP system is roughly 700 g. In orbit, we will verify whether the expected performance can be achieved under high vacuum and microgravity conditions.

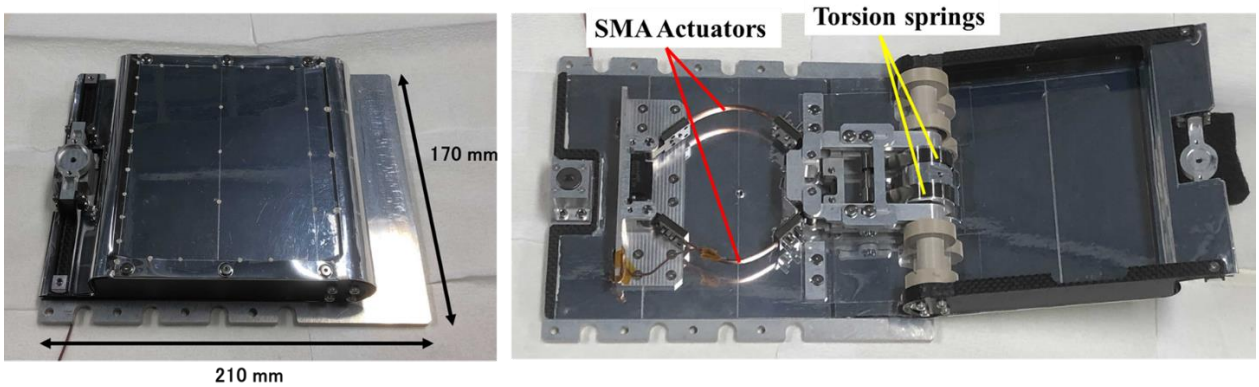


Fig. 4 Appearance of RTP (left: Stowed, right: Deployed)

## III. Configuration of thermal vacuum test evaluation

Thermal vacuum tests were conducted on a LTS, a CTS, and a RTP in order to understand the temperature response of each device to thermal loading. The temperature in the space chamber was maintained at -65 to -60 °C, and the vacuum was kept below $1.0 \times 10^{-3}$ Pa to test each device.

### A. Setup of conductivity-type thermal strap

Figure 5 shows the setup image around the conductivity-type thermal strap. The high-temperature end is bolted to an aluminum plate and heated by a heater on the other side of the plate. The low-temperature end is attached to the radiating surface via an aluminum block, and an Al-deposited polyester film is wrapped around the strap for radiation insulation. Pt1000 thermistors are used to measure the temperature, are attached with epoxy adhesive, and are connected to the control board in the ATCD for logging. The temperature was measured at three points: the heater, the hot end, and the cold end. Although two sensors were installed in the same place in the main system, the results of this test show the measurement results of the main system.

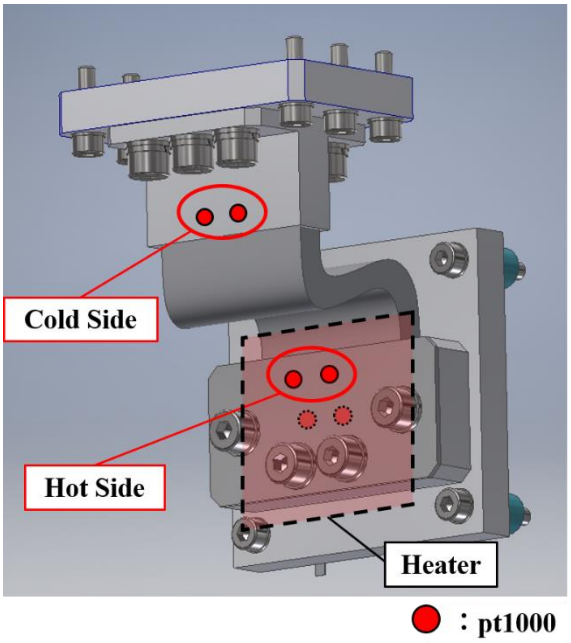


Fig. 5 Setup image of a conductivity-type thermal strap

### B. Setup of LHP-type thermal strap

Figure 6 shows the setup image around the LHP-type thermal strap. The evaporator is fixed between aluminum plates and heated by a heater on the other side of the plate. The condenser is also heated by a heater on the other side of the plate. A heater is attached to the condenser to keep the working fluid warm and to maintain the working condition under low temperature. The condenser side is attached to the heat radiation surface through an aluminum plate and a GFRP plate. An Al vapor-deposited polyester film is wrapped around the vapor and liquid tubes for radiation insulation. The temperature was measured at four points: the heater on the evaporator side, near the evaporator, at the inlet of the condenser, and at the heater on the condenser side. Although two sensors were installed in the same place in the main and auxiliary systems, the results of this test show the measurement results of the main system.

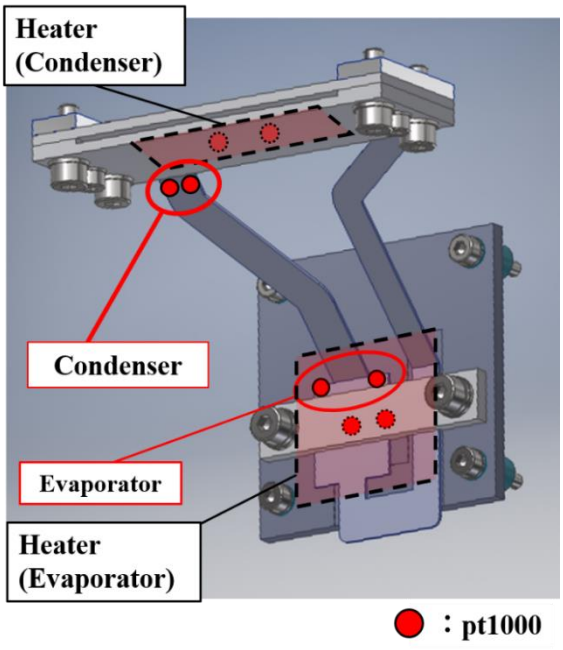


Fig. 6 Setup image of a LHP-type thermal strap

### C. Reversible thermal panel

The test setup for the performance evaluation test of the RTP is shown in Fig. 7. Unlike the two devices described above, the flexible deployment radiator was tested while it was mounted on the top of the ATCD enclosure. The temperature was measured on the heater, the fixed base of the SMA actuator (made of A5052), and the center of the back side of the fins. the Pt1000 thermistors were attached to the fixed base of the SMA actuator because they don't interfere with the operation of the SMA actuator itself. The reason why pt1000 thermistors were mounted on the fixed base of the SMA actuator was so that it would not interfere with the operation of the SMA actuator itself. Although two sensors were mounted on the same part of the main system, the results of this test show the measurement results of the main system. The radiator fin deployment angle was calculated by measuring the relative distance from the opposite SMA actuator bracket surface with an ultrasonic sensor mounted on the base side. The RTP is designed to operate by heat generated by internal devices and sunlight, so it basically requires no power. However, the RTP in the ATCD operates with heat from a heater that simulates the heat generated by internal devices, and requires 30 W of power to operate.

The inside of the space chamber during the RTP performance evaluation test is shown in Fig. 8. To prevent gravity from affecting the fin deployed and stowed, the enclosure was placed in the space chamber with the enclosure on its side as shown in Fig. 8. In order to improve the heat transfer to the end of SMA actuators, the test was conducted with a copper thin-wire braided thermal straps attached along the SMA actuators.

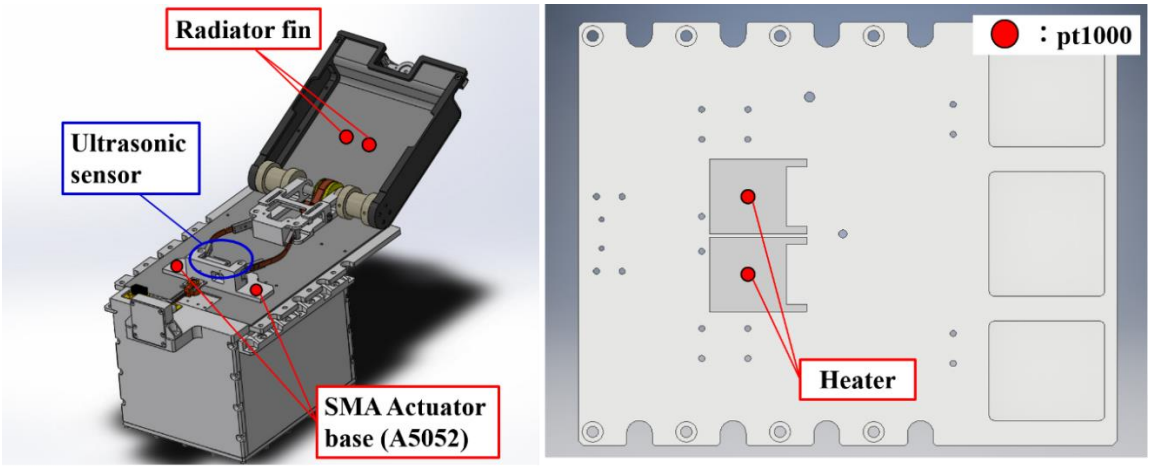


Fig. 7 Setup image of the flexible deployment radiator performance evaluation test

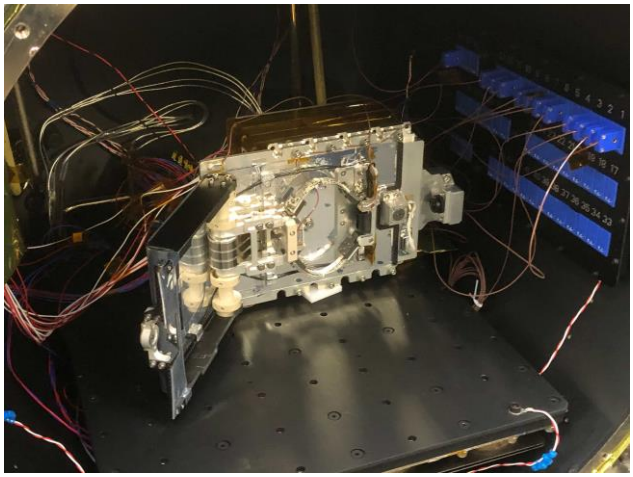

Fig. 8 View inside the space chamber during the thermal vacuum test

## IV. Experimental results and discussion

### A. Conductivity-type thermal strap

The temperature time histories of each part of the CTS during the performance evaluation test are shown in Fig. 9, and the thermal conductance between the two ends is shown in Fig. 10. In the test, the temperature of each part was measured by changing heat load in 5 W steps of 5 W, 10 W, 15 W, 10 W, and 5 W every 35 minutes. The thermal conductance between the two ends is defined by the following equation.

$$G_{GTS} = \frac{Q}{T_H - T_C} \tag{1}$$

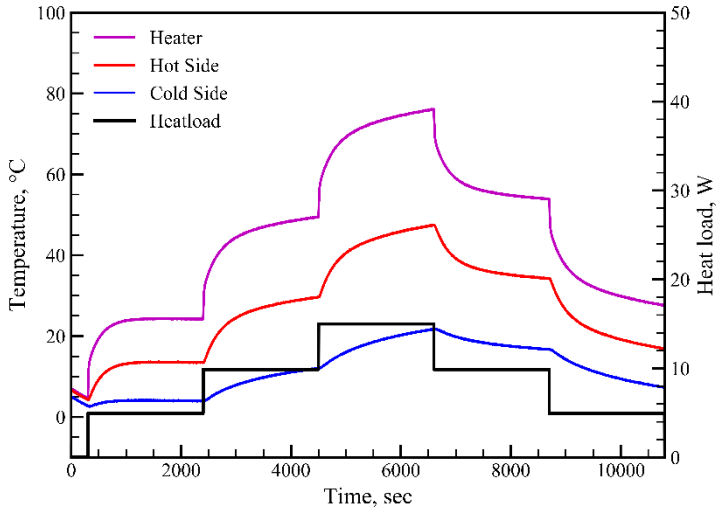


Fig. 9 Temperature Time History of CTS Performance Evaluation Test

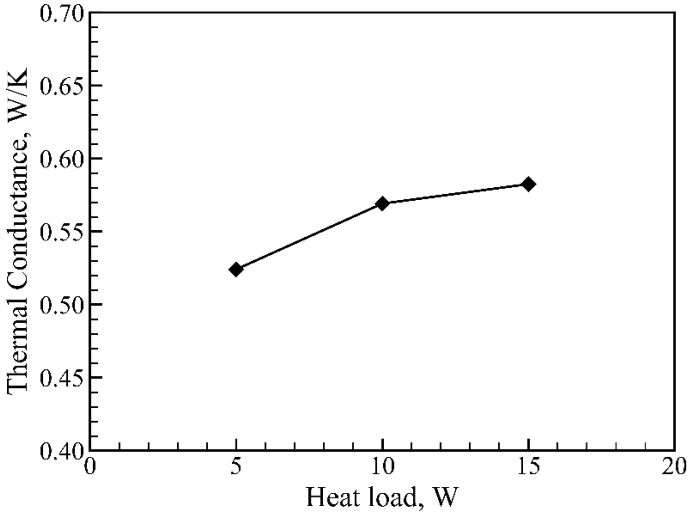


Fig. 10 Thermal Conductance between Both Ends in CTS Performance Evaluation Test

The thermal conductance between the two ends was almost constant at around 0.55 W/K regardless of the heat load. The temperature difference between the heater and the hot side is noticeable. This is considered to be due to the thermal resistance of the front and back surfaces of the CTS end caused by the small thermal conductance in the direction of the graphite sheet thickness. The temperature difference between the heater and the hot side can be estimated as the sum of the temperature difference between the front and back surfaces of the aluminum plate, the temperature difference between the aluminum plate and the CTS end, and the temperature difference between the front and back surfaces of the CTS end. Based on Fourier's law, the temperature difference between the front and back surfaces of the aluminum plate is 0.26 K, while the thermal conductivity of the graphite sheet in the thickness direction is 5 W/mK. Therefore, the temperature difference between the front and back surfaces of the CTS end is estimated to be 21.7 K. The contact heat transfer coefficient between the aluminum plate and the CTS end (contact area: 0.00114 $m^2$) is estimated to be 2100 - 2600 $W/m^2K$.

### B. LHP-type thermal strap

The temperature and time histories of the various parts in the performance evaluation test of the LTS are shown in Fig. 11. In the test, heat load on the evaporator side was increased in 0.5 W steps while the condenser was kept warm to maintain the operating condition. At 3.5 W heating on the evaporator side, the activation of the LTS (a phenomenon in which the condenser temperature rises as vapor is discharged into the transport tube after vapor generation) was confirmed. Thereafter, as heat load increased, the condenser temperature rose due to the elongation of the two-phase region, and the LTS continued to operate until the end of the test.

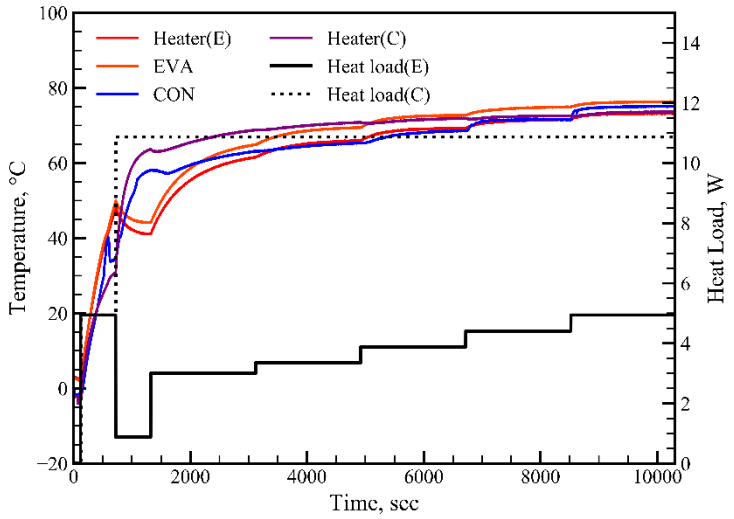


Fig. 11 Temperature time history of the LTS performance evaluation test

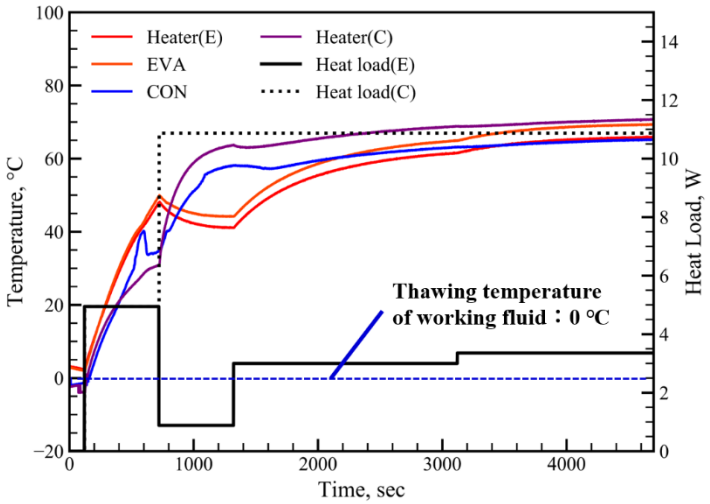


Fig. 12 Temperature time history of thawing phase in the LTS performance evaluation test

An enlarged view of the working fluid thawing phase of the LTS performance evaluation test shown in Fig. 11 is shown in Fig. 12. Immediately after heating of both sides of the evaporator and condenser began, the temperature of each part exceeded the working fluid thawing temperature: 0 °C, confirming that the working fluid was completely thawed. After thawing, the heat load was added to the evaporator side in steps of 3 W and then 0.5 W while keeping the condenser side warm. As described above, the condenser temperature followed the evaporator temperature immediately after the start of the 3.5 W load, and the LTS started up without any problems. The same LTS performance evaluation test shown in Fig. 11 was conducted several times, and no leakage of the working fluid due to repeated freezing and thawing of the working fluid, nor any degradation of the performance of the LTS was observed. Figure 13 shows the thermal conductance of the LTS during the performance evaluation tests shown in Fig. 11. The thermal conductance of the LTS, $G_{LTS}$, is defined by the following equation.

$$G_{LTS} = \frac{Q_{EVA}}{T_{EVA} - T_{CON}} \tag{2}$$

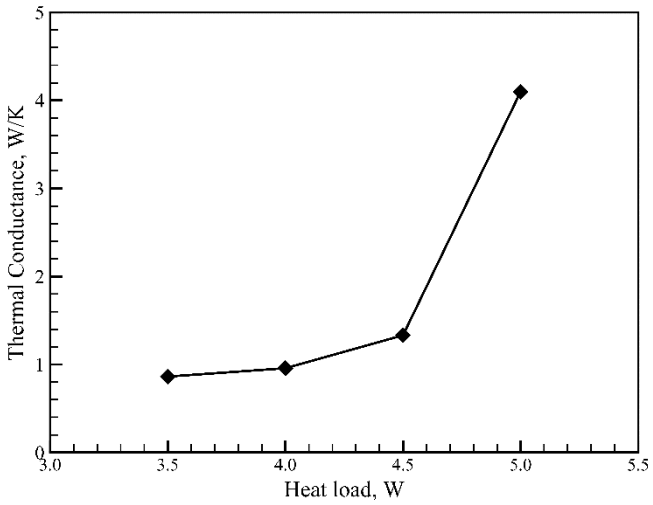


Fig. 13 Evolution of evaporator-condenser thermal conductance in the LTS performance evaluation test

As for the thermal conductance, it was confirmed that it monotonically increased as the heat load increased. In general, the temperature difference between the evaporator and the condenser in an LHP tends to decrease as heat load increases due to the extension of the two-phase region in the tube. This tendency was also confirmed in the LTS, and it can be concluded that the thermal straps, which transport heat only by heat conduction between materials, have almost constant heat transport performance regardless of the heat load, whereas the LHP-type thermal straps, which use latent heat transport of fluid, have a higher heat transport performance. On the other hand, the LHP-type thermal straps, which use latent heat transport of fluid, are expected to be effective as heat path devices especially in the configuration where the amount of heat transport is large.

### C. Reversible thermal panel

The time histories of the temperature of each part of the RTP and the radiator fin deployment angle are shown in Fig. 14, and the relationship between the base temperature of the SMA actuator and the fin deployment angle is shown in Fig. 15.

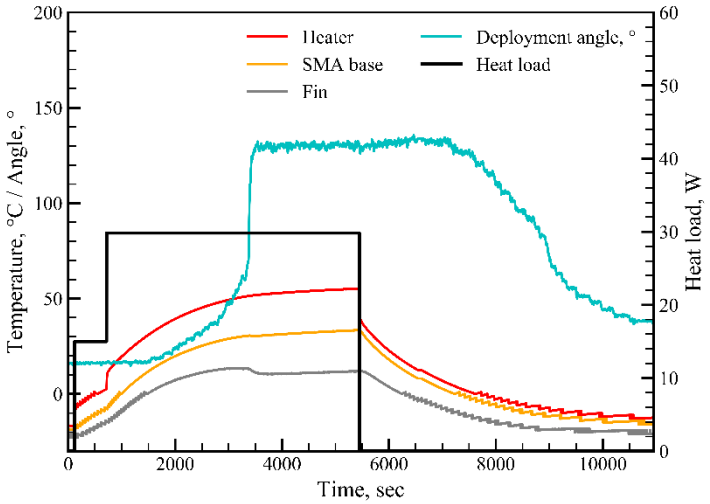


Fig. 14 Temperature time history of RTP deployment and storage test

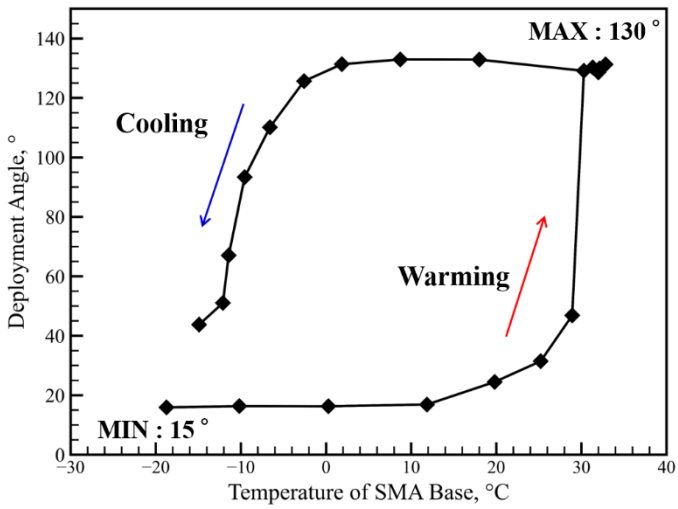


Fig. 15 Relationship between temperature and RTP fin deployment angle

As the SMA base temperature increased, the fin expansion angle gradually increased from about 15° to about 60°, and when the SMA base temperature reached 30 °C, it was confirmed that the fin deployment angle rapidly increased to about 130°. The fins began to stow when the SMA base temperature reached about 0 °C. Finally, heat load was reduced to 0 W. When the SMA base temperature reached about 0 °C, the fins began to stow, and finally, when the SMA temperature reached -15 °C, the fins stowed to about 40°. From these results, the temperature hysteresis of the SMA actuator was estimated to be about 40°C.

The on-orbit test time is set at 180 minutes, and if the test is conducted on-orbit for 90 minutes of heating and 90 minutes of cooling, the fins may not fully deploy and stow due to the lower temperature of the actual on-orbit environment. Therefore, the heating and cooling conditions need to be optimized through repeated on-orbit operations.

## V. Conclusions

The details of the elemental technologies of the advanced thermal control device; ATCD, which has been adopted as one of the demonstration themes for the rapid innovative payload demonstration satellite-2, and the results of the thermal vacuum test of ATCD components are reported. It was confirmed that the thermal conductance between the two ends of CTS was 0.50-0.55 W/K. As for LTS, it was confirmed that it could operate even after recovering from the frozen condition of the working fluid, and that there was no leakage of the working fluid and no performance degradation under vacuum environment. As the heat load increased, the thermal conductance between the evaporator and condenser increased, and finally a thermal conductance value of 4.1 W/K (at 5 W heat load) was confirmed. For RTP, it was confirmed that the radiator fins were fully expanded to 130° when the SMA actuator reached 30 ℃ during heating. On the other hand, during cooling, the temperature of the SMA actuator dropped only to -15℃, and the fins retracted only to 40°. Furthermore, the temperature hysteresis of the SMA actuator was estimated to be about 40℃ based on the experimental results.

RAISE-2 was launched in 2021 and ATCD is currently in the preparation phase for the demonstration.The demonstration test will be conducted under the same conditions as the test reported in this paper.

## VI. References

[1] JAXA, Retrieved from https://www.kenkai.jaxa.jp/eng/research/innovative/innovative.html (27.2.2022)

[2] H. Nagai, H. Tanaka, S. Kajiyama, T. Mizutani, H. Nagano, K. Sawada, K. Matsumoto, Y. Shimoda, "On-orbit demonstration of Advanced Thermal Control Devices using JAXA Rapid Innovative payload demonstration SatellitE-2 (RAISE-2)", 50th International Conference on Environmental Systems, 361, 2021.

[3] T. Mizutani, Y. Machida, H. Nagano, " Verification of Heat Transport Characteristics for Space Demonstration of Ultra-Thin Loop Heat Pipe for Innovative Thermal Control Device Installation", Proceedings of the 41st Japan Symposium on Thermophysical Properties B112, 2020.

[4] S. Ohno, H. Nagano, S. Tachikawa, H. Ogawa, and Y. Nishikawa, "Study on an Advanced Deployable Radiator with High-Thermal-Conductive Graphite Sheets for Small Satellites", Journal of Thermophysics and Heat Transfer, Vol. 29, No. 2, pp. 403-411, 2015.

[5] KANEKA Corporation, Retrieved from https://www.kaneka.co.jp/en/business/qualityoflife/eit_003.html (27.2.2022)

[6] SHINKO ELECTRIC INDUSTRIES CO., LTD., Retrieved from https://www.shinko.co.jp/english/product/under-development/m3hp/ (27.2.2022).